European Journal of Medicinal Chemistry 44 (2009) 2482–2496

Contents lists available at ScienceDirect

European Journal of Medicinal Chemistry

journal homepage: http://www.elsevier.com/locate/ejmech

Original article

Development of CoMFA and CoMSIA models of affinity and selectivity for indole ligands of cannabinoid CB1 and CB2 receptors

Guilherme B.L. De Freitas [a,b], Leandro L. da Silva [a], Nelilma C. Romeiro [a], Carlos A.M. Fraga [a,b,*]

[a] Laboratório de Avaliação e Síntese de Substâncias Bioativas (LASSBio), Faculdade de Farmácia, Universidade Federal do Rio de Janeiro (UFRJ), Rio de Janeiro, P.O. Box 68023, Rio de Janeiro 21941-902, Brazil
[b] Programa de Pós-Graduação em Química, Instituto de Química, Universidade Federal do Rio de Janeiro (UFRJ), Rio de Janeiro, Rio de Janeiro 21941-909, Brazil

ARTICLE INFO

Article history:
Received 5 August 2008
Received in revised form
17 December 2008
Accepted 15 January 2009
Available online 3 February 2009

Keywords:
Cannabinoid receptors
3D-QSAR
CoMFA selectivity model
CoMFA affinity model
CoMSIA
Indole ligands
CB1 receptor
CB2 receptor

ABSTRACT

This paper describes CoMFA and CoMSIA studies for affinity and selectivity of a series of indole ligands to cannabinoid CB1 and CB2 receptors. The developed models have proven to be predictive, with average q^2 of 0.675 and average r^2 of 0.855, demonstrating a good statistical validation. The obtained results have helped us to understand the structural motifs that are responsible for the affinity and selectivity of some of these derivatives towards each subtype of cannabinoid receptor and have demonstrated that the exploited 3D-QSAR methods could be useful tools for the design of new safer analogues presenting better affinity and selectivity profiles.

1. Introduction

The emerging role of the lipid signaling endocannabinoid system in the regulation of several central or peripheral physiological functions has stimulated the search of new therapeutically useful tools able to modulate it selectively at bioreceptor level, as agonists or antagonists. At present, two cannabinoid receptor types, denoted as CB1 and CB2, have been determined and the distinction between them is based on the differences in their amino acid sequences, their signaling mechanisms, and their tissue distribution [1].

Recent publications have demonstrated that the orphan receptor GPR55 responds to a similar series of fatty-acid ethanolamides and related compounds as do the cannabinoid receptors [2,3]. Regarding their distribution and functionality, CB1 receptors are predominantly located in the central nervous system, and they are probably responsible for most of the overt pharmacological effects of cannabinoid ligands [4–6]. The CB2 receptor is found in peripheral tissues, such as spleen, tonsils and immunocytes [7].

Both CB1 and CB2 are seven-transmembrane (7TM) receptors that belong to the rhodopsin-like family class A of G-protein coupled receptors (GPCRs) and control a wide variety of multiple intracellular signal transduction pathways. GPCRs are important targets for drug discovery. Till date, over 30% of the clinically marketed drugs are active at this receptor family. GPCRs are integral membrane proteins that characteristically have seven R-helices spanning a membrane bridged by three intracellular and three extracellular loops [8].

Cannabinoid receptor agonists can be divided into four structurally distinct classes of compounds (Fig. 1). These include classical cannabinoids, like Δ^9-tetrahydrocannabinol (Δ^9-THC, **1**) as the principal psychoactive constituent of marijuana, non-classical cannabinoids developed by Pfizer, represented by DMH = 1,1-dimethylheptyl (CP-55,940, **2**), aminoalkylindoles, such as WIN-55,212-2 (**3**) considered to be the first example of this class of cannabinoid receptor ligands, and endogenous cannabinoids such as arachidonylethanolamide, also called anandamide (AEA, **4**) [9].

Both CB1 and CB2 agonists inhibit adenyl cyclase by activation of a pertussis toxin-sensitive G-protein [10]. Moreover CB1 activation inhibits some types of calcium channels and activates inwardly

* Corresponding author. Laboratório de Avaliação e Síntese de Substâncias Bioativas (LASSBio), Faculdade de Farmácia, Universidade Federal do Rio de Janeiro (UFRJ), Rio de Janeiro, P.O. Box 68023, RJ 21941-902, Brazil. Tel.: +55 21 2562 6503; fax: +55 21 2562 6478.
E-mail address: cmfraga@pharma.ufrj.br (C.A.M. Fraga).

0223-5234/$ – see front matter © 2009 Elsevier Masson SAS. All rights reserved.
doi:10.1016/j.ejmech.2009.01.026

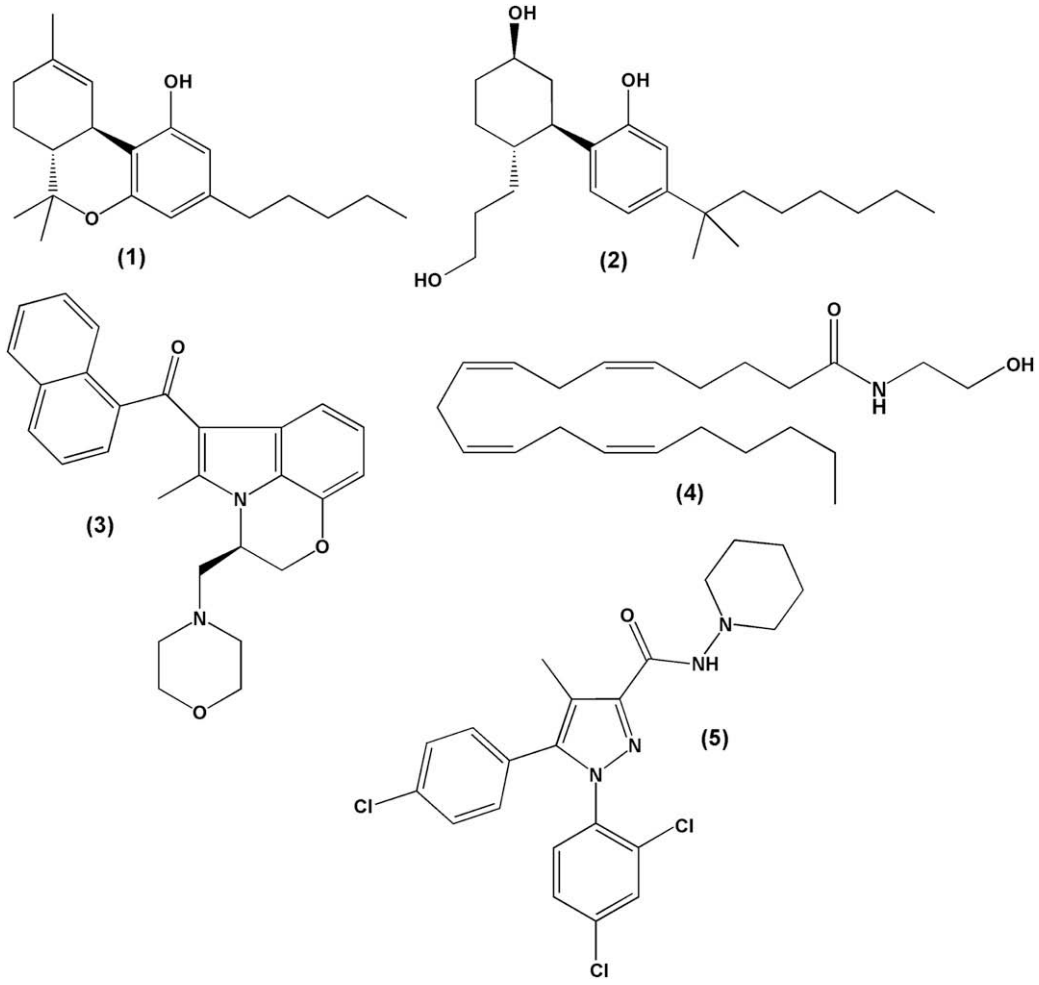

Fig. 1. Molecular structures of representative cannabinoid agonists (**1**–**4**) and antagonist (**5**).

rectifying potassium channels [9,11]. Cannabinoid agonists have been suggested to have potential therapeutic uses as appetite stimulants in wasting syndromes, as analgesics, as anti-emetics for the attenuation of the nausea and vomiting in cancer chemotherapy, as antidiarrheals for decreased intestinal motility, as antispasmodics for relief from muscle spasms/spasticity in multiple sclerosis, as anti-proliferative agents of glioma growth, as anti-glaucoma agents for reduction of intraocular pressure and as agents for the treatment of diseases associated with inappropriate retention of aversive memories such as post-traumatic stress disorders and phobias [12–16]. Untoward side effects accompanying cannabinoid agonist therapeutic responses include alterations in cognition and memory, dysphoria/euphoria, and sedation [17]. During the last decade there has been a growing interest towards the modulation of the cannabinoid CB1 receptor. The identification of CB1 cannabinoid receptor antagonists has been one of the major advances in cannabinoid research, since the discovery of the first cannabinoid receptor antagonist, rimonabant (SR-141716A) by Sanofi in 1994 [18]. Thus, the development of these ligands has opened new therapeutic applications.

Aminoalkylindole (**1**) derivatives are structurally dissimilar from other agonist classes, and site-directed mutagenesis has revealed that the amino acids set important for their binding differs significantly from those of the other classes of ligands, indicating that the binding site of this kind of ligand is probably different from the other agonists [11]. Regarding the CB1 receptor more specifically, mutation studies have reported that a K3.28(192)A mutation results in a greater loss in affinity for AEA (**4**) and CP-55,940 (**2**), while the affinity of WIN-55,212-2 (**3**) remains unchanged [19]. Additionally, the mutation of F3.36(191)A, W5.43(279)A, and W6.48(356)A in the CB1 receptor determined a loss of affinity only for WIN-55,212-2 (**3**), whereas the AEA (**4**) and CP-55,940 (**2**) affinities were unaffected [20]. Regarding the CB2 receptor, Song and co-workers reported that the mutation of F5.46(197)V determined a 14-fold decrease in CB2 affinity for WIN-55,212-2 (**3**), while the CP-55,940 (**2**) and AEA (**4**) affinities were unaltered [21].

The knowledge of the 3D structure of cannabinoid receptors could be of great help in the task of understanding their function and in the rational design of specific and selective ligands. So far, many computational 3D-QSAR [22–31], homology modeling and docking studies [20–34] with cannabinoid ligands have been carried out on CB1 and CB2 receptors. Among the 3D-QSAR studies described in the literature, there are models for classic, non-classic, endocannabinoid, pyrazole and indole ligands. Nevertheless, none of these studies have addressed models of affinity *and* selectivity of ligands towards both subtypes of receptors (CB1 and CB2) using 3D-QSAR methods. According to Song et al. [19,21] and McAllister et al. [20] studies the indole derivatives bind in a different place within the active sites of CB1 and CB2 compared to the other classes of agonists (classic cannabinoids, non-classic ligands and endocannabinoids). Following these results, in the present study, comparative molecular field analysis (CoMFA) and comparative

Table 1
Molecular structures, binding affinity (p*Ki*) and CB1/CB2 p*Ki* ratio of indole analogues used in the construction of CoMFA and CoMSIA models. The molecules used as test set are highlighted with an asterisk (*).

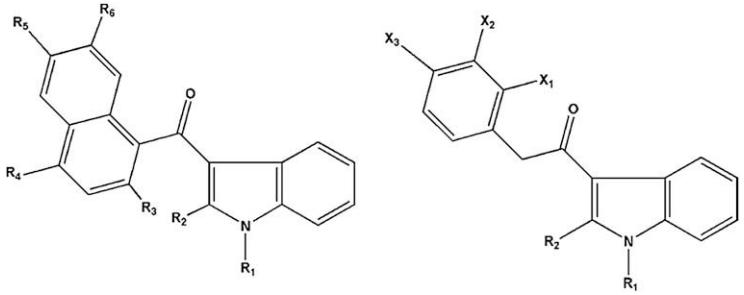

Compound	R_1	R_2	R_3	R_4	R_5	R_6	X_1	X_2	X_3	CB1	CB2	CB1/CB2 p*Ki* ratio
1) JWH-007	nC_5H_{11}	CH_3	H	H	H	H	–	–	–	8.022	8.538	0.940
2) JWH-015	nC_3H_7	CH_3	H	H	H	H	–	–	–	6.785	7.860	0.863
3) JWH-018*	nC_5H_{11}	H	H	H	H	H	–	–	–	8.045	8.538	0.942
4) JWH-046	nC_3H_7	CH_3	H	H	H	CH_3	–	–	–	6.464	7.796	0.829
5) JWH-048	nC_5H_{11}	CH_3	H	H	H	CH_3	–	–	–	7.970	9.310	0.856
6) JWH-072	nC_3H_7	H	H	H	H	H	–	–	–	5.978	6.770	0.883
7) JWH-076	nC_3H_7	H	H	H	H	CH_3	–	–	–	6.669	6.975	0.956
8) JWH-079	nC_3H_7	H	H	OCH_3	H	H	–	–	–	7.200	7.495	0.961
9) JWH-081	nC_5H_{11}	H	H	OCH_3	H	H	–	–	–	8.920	7.907	1.128
10) JWH-094	nC_3H_7	CH_3	H	OCH_3	H	H	–	–	–	6.322	7.013	0.901
11) JWH-098	nC_5H_{11}	CH_3	H	OCH_3	H	H	–	–	–	8.346	8.721	0.957
12) JWH-120	nC_3H_7	H	H	CH_3	H	H	–	–	–	5.977	8.215	0.728
13) JWH-122	nC_5H_{11}	H	H	CH_3	H	H	–	–	–	9.161	8.921	1.027
14) JWH-148	nC_3H_7	CH_3	H	CH_3	H	H	–	–	–	6.910	7.854	0.880
15) JWH-149*	nC_5H_{11}	CH_3	H	CH_3	H	H	–	–	–	8.301	9.137	0.909
16) JWH-153*	nC_5H_{11}	CH_3	H	H	OCH_3	H	–	–	–	6.602	7.959	0.830
17) JWH-159	nC_5H_{11}	CH_3	H	H	H	OCH_3	–	–	–	7.346	7.983	0.920
18) JWH-160	nC_3H_7	CH_3	H	H	H	OCH_3	–	–	–	5.804	6.356	0.913
19) JWH-163	nC_3H_7	H	H	H	OCH_3	H	–	–	–	5.627	6.860	0.820
20) JWH-164	nC_5H_{11}	H	H	H	H	OCH_3	–	–	–	8.180	8.161	1.002
21) JWH-165	nC_3H_7	H	H	H	H	OCH_3	–	–	–	6.690	7.149	0.936
22) JWH-166*	nC_5H_{11}	H	H	H	OCH_3	H	–	–	–	7.356	8.721	0.843
23) JWH-180	nC_3H_7	H	H	nC_3H_7	H	H	–	–	–	7.585	8.018	0.946
24) JWH-181	nC_5H_{11}	CH_3	H	nC_3H_7	H	H	–	–	–	8.886	9.208	0.965
25) JWH-182*	nC_5H_{11}	H	H	nC_3H_7	H	H	–	–	–	9.187	8.959	1.025
26) JWH-189	nC_3H_7	CH_3	H	nC_3H_7	H	H	–	–	–	7.283	7.921	0.919
27) JWH-210	nC_5H_{11}	H	H	C_2H_5	H	H	–	–	–	9.337	9.161	1.019
28) JWH-211	nC_3H_7	CH_3	H	C_2H_5	H	H	–	–	–	7.154	7.921	0.903
29) JWH-212	nC_3H_7	H	H	C_2H_5	H	H	–	–	–	7.481	8.000	0.935
30) JWH-213	nC_5H_{11}	CH_3	H	C_2H_5	H	H	–	–	–	8.823	9.377	0.941
31) JWH-234	nC_5H_{11}	H	H	H	H	C_2H_5	–	–	–	8.075	8.420	0.959
32) JWH-235	nC_3H_7	H	H	H	H	C_2H_5	–	–	–	6.471	6.910	0.936
33) JWH-236	nC_3H_7	CH_3	H	H	H	C_2H_5	–	–	–	5.869	6.620	0.887
34) JWH-239	nC_3H_7	H	H	nC_4H_9	H	H	–	–	–	6.465	7.284	0.888
35) JWH-240	nC_5H_{11}	H	H	nC_4H_9	H	H	–	–	–	7.853	8.143	0.964
36) JWH-241	nC_3H_7	CH_3	H	nC_4H_9	H	H	–	–	–	6.832	7.310	0.935
37) JWH-242	nC_5H_{11}	CH_3	H	nC_4H_9	H	H	–	–	–	7.376	8.187	0.901
38) JWH-258	nC_5H_{11}	H	H	OC_2H_5	H	H	–	–	–	8.337	7.979	1.045
39) JWH-259*	nC_3H_7	H	H	OC_2H_5	H	H	–	–	–	6.657	7.131	0.934
40) JWH-260	nC_5H_{11}	CH_3	H	OC_2H_5	H	H	–	–	–	7.537	7.602	0.991
41) JWH-261	nC_3H_7	CH_3	H	OC_2H_5	H	H	–	–	–	6.115	6.656	0.919
42) JWH-262	nC_5H_{11}	CH_3	H	H	H	C_2H_5	–	–	–	7.552	8.252	0.915
43) JWH-265	nC_3H_7	H	OCH_3	H	H	H	–	–	–	5.421	7.097	0.764
44) JWH-267	nC_5H_{11}	H	OCH_3	H	H	H	–	–	–	6.419	8.143	0.788
45) JWH-268*	nC_5H_{11}	CH_3	OCH_3	H	H	H	–	–	–	5.860	7.398	0.792
46) JWH-167	nC_5H_{11}	H	–	–	–	–	H	H	H	7.045	6.799	1.036
47) JWH-201	nC_5H_{11}	H	–	–	–	–	H	H	OCH_3	5.973	6.352	0.940
48) JWH-202*	nC_5H_{11}	CH_3	–	–	–	–	H	H	OCH_3	5.775	6.190	0.933
49) JWH-203	nC_5H_{11}	H	–	–	–	–	Cl	H	H	8.096	8.154	0.993
50) JWH-204	nC_5H_{11}	CH_3	–	–	–	–	Cl	H	H	7.886	7.602	1.037
51) JWH-205*	nC_5H_{11}	CH_3	–	–	–	–	H	H	H	6.906	6.744	1.024
52) JWH-206*	nC_5H_{11}	H	–	–	–	–	H	H	Cl	6.410	6.302	1.017
53) JWH-207	nC_5H_{11}	CH_3	–	–	–	–	H	H	Cl	5.796	5.429	1.068
54) JWH-208	nC_5H_{11}	H	–	–	–	–	H	H	CH_3	6.747	6.244	1.081
55) JWH-209	nC_5H_{11}	CH_3	–	–	–	–	H	H	CH_3	6.127	5.868	1.044
56) JWH-237	nC_5H_{11}	H	–	–	–	–	H	Cl	H	7.420	6.974	1.064
57) JWH-248*	nC_5H_{11}	H	–	–	–	–	H	H	Br	5.988	6.182	0.969
58) JWH-249	nC_5H_{11}	H	–	–	–	–	Br	H	H	8.075	7.698	1.049
59) JWH-250	nC_5H_{11}	H	–	–	–	–	OCH_3	H	H	7.958	7.481	1.064
60) JWH-251	nC_5H_{11}	H	–	–	–	–	CH_3	H	H	7.537	6.835	1.103

Table 1 (*continued*)

Compound	R_1	R_2	R_3	R_4	R_5	R_6	X_1	X_2	X_3	CB1	CB2	CB1/CB2 p*K*i ratio
61) JWH-252*	nC_5H_{11}	CH_3	–	–	–	–	CH_3	H	H	7.638	7.721	0.989
62) JWH-253	nC_5H_{11}	CH_3	–	–	–	–	H	OCH_3	H	7.207	7.075	1.019
63) JWH-302	nC_5H_{11}	H	–	–	–	–	H	OCH_3	H	7.769	7.050	1.102
64) JWH-303	nC_5H_{11}	CH_3	–	–	–	–	H	Cl	H	6.931	6.860	1.010
65) JWH-305	nC_5H_{11}	CH_3	–	–	–	–	Br	H	H	7.823	7.537	1.038
66) JWH-306*	nC_5H_{11}	CH_3	–	–	–	–	OCH_3	H	H	7.602	7.086	1.073
67) JWH-311	nC_5H_{11}	H	–	–	–	–	F	H	H	7.638	7.408	1.031
68) JWH-312*	nC_5H_{11}	H	–	–	–	–	H	F	H	7.142	7.040	1.014
69) JWH-313	nC_5H_{11}	H	–	–	–	–	H	H	F	6.374	6.437	0.990
70) JWH-314	nC_5H_{11}	CH_3	–	–	–	–	F	H	H	7.408	7.119	1.041
71) JWH-315	nC_5H_{11}	CH_3	–	–	–	–	H	F	H	6.366	6.739	0.945

molecular similarity indices analysis (CoMSIA) 3D-QSAR models of affinity and selectivity of a series of indole ligands for the cannabinoid receptors CB1 and CB2 were built and refined. The developed 3D-QSAR models correlate variations in the affinity and selectivity for both subtypes of receptors using 71 indole derivatives previously described in the literature [35–37].

2. Methods

2.1. Data set selection

The data set used in this study was chosen from a series of ligands with both CB1 and CB2 receptor affinities. Literature was reviewed and we selected only those publications where the binding affinity of these compounds was measured by pharmacological protocols with the same radioligand, the non-classical cannabinoid, CP-55,940 (**2**). However CB1 was tested in homogenates of rat brain [38] and CB2 in preparations of cloned human receptors [39]. The structurally related indole analogues selected to compose our database could be split into two groups, those presenting a substituted naphthyl α-carbonyl group attached to position 3 of the heterocyclic ring (Table 1) and some simplified analogues presenting substituted benzylcarbonyl groups at C-3 (Table 1). The affinity of all the 71 compounds used in this study was measured as *K*i and was expressed in negative logarithmic units, −log *K*i or p*K*i (Table 1). The training and the test sets represented by 56 and 15 compounds (Table 1), respectively, were selected randomly [35–37], and the distribution of CB1 and CB2 p*K*i values for the training and test sets is shown in Fig. 2. The elected indole ligands showed good structural variation and affinities (p*K*i) ranging from 5.627 to 9.376 and 5.429 to 9.376 (Fig. 2) for the CB1 and CB2 receptors, respectively, making them suitable for 3D-QSAR studies.

2.2. Molecular modeling

2.2.1. General procedures

Initially, the structures were built using PC Spartan Pro 1.0 for Windows XP [40], and the conformer distribution of each one was calculated by molecular mechanics with the Merck molecular force field (MMFF) [41]. Subsequently, the lowest-energy conformation found for each structure was submitted to optimization with the semi empirical AM1 method. This energy was then compared with that obtained from the conformation previously described in the literature [32,20] as the bioactive conformation, using the single point energy by AM1. 3D-QSAR studies were performed using SYBYL software version 7.3 [42]. For further calculations with CoMFA/CoMSIA, Gasteiger–Hückel charges were also assigned to all molecules using SYBYL.

2.3. Alignment of molecules

One of the most important adjustable parameters in CoMFA is the relative alignment of all the compounds to one another so that they have a comparable conformation and a similar orientation of pharmacophoric groups in space. In agreement to Akamatsu's guidelines [43] the proposed alignment for the studied compounds has been done following their common pharmacophores. In this study, the most active molecule of the database (JWH-210, **27**) was used as a template for superimposition, assuming that its bioactive conformation represents the most probable conformation of the indole analogues at the putative receptor [32,20]. Two atom-based alignments were manually carried out using the Fit Atoms tool in SYBYL 7.3 software. (a) Alignment 1: atoms 1, 3 and 5 of the indole ring, the carbonylic carbon and atom 1′ of the naphthyl ring were selected and highlighted (Fig. 3); (b) Alignment 2: 7 atoms were selected for the alignment of all compounds. These atoms are also

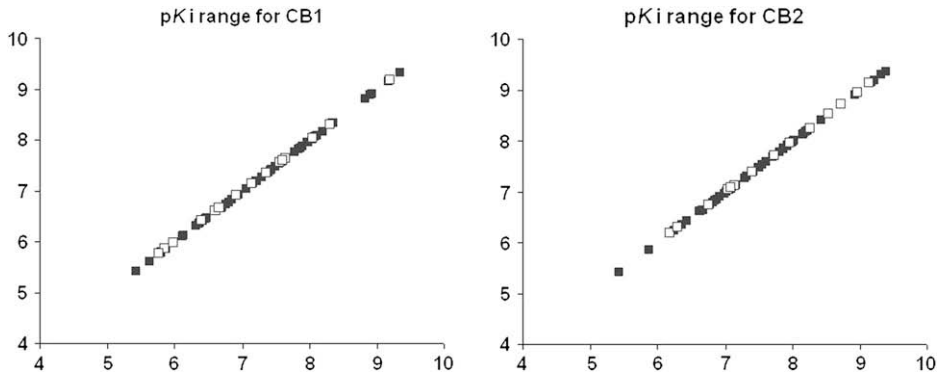

Fig. 2. Distribution of binding affinity (p*K*i) values of the molecules used to compose the training and the test sets for CB1 and CB2 receptors. The 56 compounds elected as training set are highlighted in black and the 15 compounds used as test set are highlighted in white.

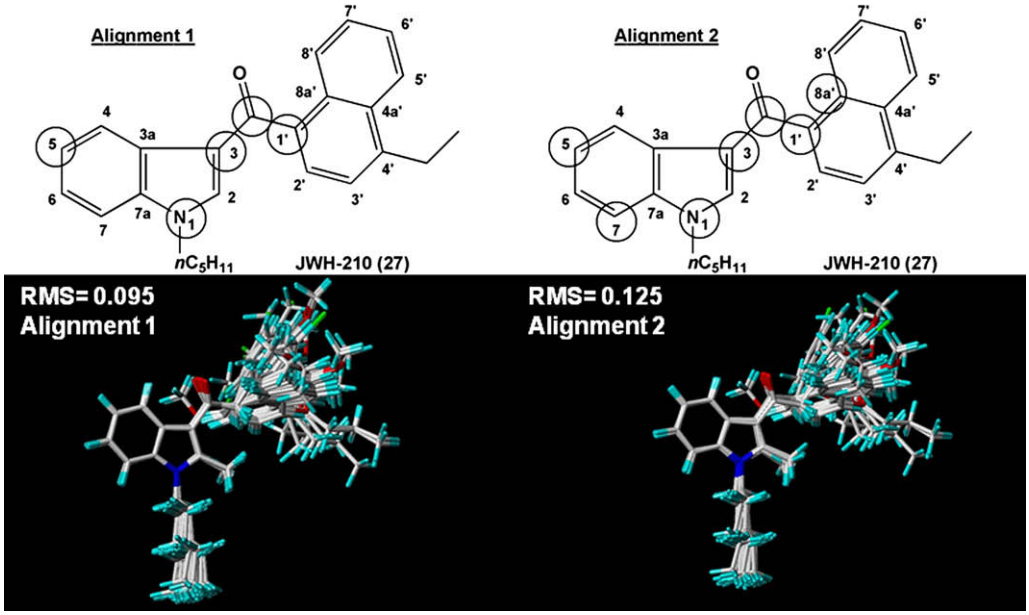

Fig. 3. Atom definition and superposition of the indole analogues following alignments 1 and 2.

highlighted in Fig. 3 and include not only atoms previously selected for the alignment 1 but also atoms 7 and 8a′ of the indole and naphthyl rings, respectively. JWH-210 (**27**) was used as the reference compound for atom numbering (Table 1) and its graphical representation depicts the best root-mean-square (RMS) value obtained with alignment 1, which justifies its use in the study.

2.4. CoMFA studies

CoMFA studies were performed with the QSAR module of SYBYL 7.3 program for each combination of steric and electrostatic molecular fields, which were sampled at each point of regularly spaced grids of 1.0, 1.5, and 2.0 Å. The steric and electrostatic fields were calculated using the default probe, an sp^3 carbon atom with a charge of +1. CoMFA calculates steric fields using a Lennard-Jones potential and electrostatic field using a Coulomb potential [44]. Different cutoff combinations of the steric and electrostatic fields were tested (Table 2).

2.5. CoMSIA studies

In the CoMSIA methodology, the alignment that generated the most predictive CoMFA models was used. Also, five physicochemical properties, k (steric, electrostatic, hydrophobic, and hydrogen-bond donor and acceptor) were evaluated using a Gaussian function. The steric/electrostatic, hydrophobic, hydrogen-bond donor and acceptor contributions were calculated separately. The attenuation factor was set at the default value of 0.3.

Table 2
Different cutoff combinations of the steric and electrostatic fields applied in the development of the 3D-QSAR models for indole ligands of cannabinoid receptors.

Steric (kcal mol^{-1})	Electrostatic (kcal mol^{-1})
30.00	30.00
35.00	30.00
30.00	35.00
25.00	30.00
30.00	25.00
20.00	30.00
30.00	20.00
25.00	35.00
35.00	25.00
40.00	30.00
30.00	40.00

2.6. PLS analysis

CoMFA field values for the training set were correlated with affinity (p*K*i) and selectivity (CB1/CB2 or CB2/CB1 p*K*i ratio) values using PLS. The optimum number of components to use was determined by leave-one-out cross-validation (LOO) [41] using a maximum of 10 principal components for each response at a time. To avoid over fitted 3D-QSAR, the optimum number of components (*N*) used in the model derivation was chosen from the analysis with the highest q^2 value for the training set. This procedure speeds up analysis and reduces noise. In the above stage, the robustness of the 'best' correlation model was determined.

Table 3
Statistical results for the best CoMFA and CoMSIA models of affinity towards CB1 and CB2 receptors obtained for the training set and test set.

	q^2 [a]	N[b]	SEP[c]	r^2 [d]	SEE[e]	F[f]	r^2_{pred}[g]
CB1							
CoMFA std	0.785	6	0.472	0.926	0.276	102.532	0.909
CoMSIA steric + electrostatic	0.743	7	0.521	0.908	0.312	67.681	0.820
CoMSIA hydrophobic	0.716	6	0.554	0.907	0.317	57.230	0.406
CB2							
CoMFA std	0.751	6	0.455	0.898	0.293	71.707	0.901
CoMSIA steric + electrostatic	0.755	5	0. 449	0.869	0.328	66.452	0.812
CoMSIA hydrophobic	0.713	5	0.486	0.868	0.329	65.998	0.782

[a] Cross-validation correlation coefficient.
[b] Number of components.
[c] Standard error of prediction.
[d] Correlation coefficient.
[e] Standard error of estimation.
[f] *F*-ratio.
[g] Correlation coefficient between the observed and predictive activities of the test set.

Table 4
Observed and predicted binding affinity values, given in p*Ki* (p*Ki* = −log [*Ki*]) obtained by applying the CoMFA (steric/electrostatic) and CoMSIA (hydrophobic) models for cannabinoid CB1 and CB2 receptor ligands and the difference between the observed *versus* CoMFA and CoMSIA predicted binding affinity values towards CB1 and CB2 receptors.

Compound	[a]CB1	[a]CB1	[d]CB1	[c]CB1	[e]CB1	[a]CB2	[b]CB2	[d]CB2	[c]CB2	[a]CB2
1) JWH-007	8.022	7.819	0.203	7.952	0.070	8.538	8.559	−0.021	8.619	−0.081
2) JWH-015	6.785	6.087	0.698	6.265	0.520	7.860	7.244	0.616	7.378	0.482
3) JWH-018*	8.045	8.242	−0.197	8.417	−0.372	8.538	8.510	0.028	8.683	−0.145
4) JWH-046	6.464	6.153	0.311	6.229	0.235	7.796	7.462	0.334	7.291	0.505
5) JWH-048	7.970	7.886	0.084	7.917	0.053	9.310	8.777	0.533	8.533	0.777
6) JWH-072	5.978	6.510	−0.532	6.730	−0.752	6.770	7.195	−0.425	7.441	−0.671
7) JWH-076	6.669	6.576	0.093	6.694	−0.025	6.975	7.416	−0.441	7.355	−0.380
8) JWH-079	7.200	7.170	0.030	6.861	0.339	7.495	7.091	0.404	7.052	0.443
9) JWH-081	8.920	8.903	0.017	8.549	0.371	7.907	8.406	−0.499	8.294	−0.387
10) JWH-094	6.322	6.486	−0.164	6.314	0.008	7.013	7.086	−0.073	6.995	0.018
11) JWH-098	8.346	8.229	0.117	7.996	0.350	8.721	8.442	0.279	8.235	0.486
12) JWH-120	5.977	7.019	−1.042	7.109	−1.132	8.215	7.889	0.326	7.942	0.273
13) JWH-122	9.161	8.752	0.409	8.797	0.364	8.921	9.204	−0.283	9.183	−0.262
14) JWH-148	6.910	6.595	0.315	6.645	0.265	7.854	7.936	−0.082	7.878	−0.024
15) JWH-149*	8.301	8.328	−0.027	8.332	−0.031	9.137	9.251	−0.114	9.120	0.017
16) JWH-153*	6.602	7.324	−0.722	7.510	−0.908	7.959	8.464	−0.505	8.392	−0.433
17) JWH-159	7.346	7.522	−0.176	7.392	−0.046	7.983	7.880	0.103	7.850	0.133
18) JWH-160	5.804	5.787	0.017	5.762	0.042	6.356	6.515	−0.159	6.630	−0.274
19) JWH-163	5.627	5.722	−0.095	5.778	−0.151	6.860	7.101	−0.241	6.754	0.106
20) JWH-164	8.180	8.144	0.036	8.309	−0.129	8.161	8.141	0.020	8.026	0.135
21) JWH-165	6.690	6.608	0.082	6.539	0.151	7.149	7.014	0.135	6.765	0.384
22) JWH-166*	7.356	7.251	0.105	7.626	−0.270	8.721	8.229	0.492	8.052	0.669
23) JWH-180	7.585	7.204	0.381	7.414	0.171	8.018	7.785	0.233	7.116	0.902
24) JWH-181	8.886	8.902	−0.016	7.366	1.520	9.208	9.105	0.103	7.908	1.300
25) JWH-182*	9.187	8.937	0.250	8.921	0.266	8.959	9.099	−0.140	9.123	−0.164
26) JWH-189	7.283	7.163	0.120	9.053	−1.770	7.921	7.958	−0.037	9.149	−1.228
27) JWH-210	9.337	9.306	0.031	7.264	2.073	9.161	9.259	−0.098	8.084	1.077
28) JWH-211	7.154	7.172	−0.018	5.963	1.191	7.921	8.143	−0.222	6.883	1.038
29) JWH-212	7.481	7.494	−0.013	5.405	2.076	8.000	8.121	−0.121	6.789	1.211
30) JWH-213	8.823	8.804	0.019	7.836	0.987	9.377	9.484	−0.107	7.624	1.753
31) JWH-234	8.075	8.182	−0.107	8.183	−0.108	8.420	8.387	0.033	7.417	1.003
32) JWH-235	6.471	6.449	0.022	6.722	−0.251	6.910	7.073	−0.163	6.738	0.172
33) JWH-236	5.869	6.025	−0.156	6.230	−0.361	6.620	7.118	−0.498	5.427	1.193
34) JWH-239	6.465	6.407	0.058	5.830	0.635	7.284	7.037	0.247	5.361	1.923
35) JWH-240	7.853	7.810	0.043	6.655	1.198	8.143	8.087	0.056	6.024	2.119
36) JWH-241	6.832	6.915	−0.083	6.254	0.578	7.310	7.000	0.310	5.957	1.353
37) JWH-242	7.376	7.473	−0.097	9.299	−1.923	8.187	8.130	0.057	9.087	−0.900
38) JWH-258	8.337	8.291	0.046	7.458	0.879	7.979	7.898	0.081	8.149	−0.170
39) JWH-259*	6.657	6.902	−0.245	7.362	−0.705	7.131	7.114	0.017	7.963	−0.832
40) JWH-260	7.537	8.057	−0.520	8.586	−1.049	7.602	8.140	−0.538	9.141	−1.539
41) JWH-261	6.115	6.275	−0.160	8.118	−2.003	6.656	6.735	−0.079	8.218	−1.562
42) JWH-262	7.552	8.021	−0.469	6.430	1.122	8.252	8.573	−0.321	6.976	1.276
43) JWH-265	5.421	5.238	0.183	5.965	−0.544	7.097	6.769	0.328	6.912	0.185
44) JWH-267	6.419	6.649	−0.230	7.550	−1.131	8.143	7.937	0.206	6.931	1.212
45) JWH-268*	5.860	6.313	−0.453	6.283	−0.423	7.398	7.922	−0.524	7.086	0.312
46) JWH-167	7.045	7.211	−0.166	7.928	−0.883	6.799	7.119	−0.320	8.220	−1.421
47) JWH-201	5.973	5.572	0.401	6.910	−0.937	6.353	6.071	0.282	7.496	−1.143
48) JWH-202*	5.775	5.540	0.235	7.524	−1.749	6.190	6.059	0.131	8.157	−1.967
49) JWH-203	8.096	8.049	0.047	8.881	−0.785	8.155	7.734	0.421	7.011	1.144
50) JWH-204	7.886	7.582	0.304	8.165	−0.279	7.602	7.161	0.441	7.961	−0.359
51) JWH-205*	6.906	7.128	−0.222	7.511	−0.605	6.745	7.166	−0.421	7.088	−0.343
52) JWH-206*	6.410	6.457	−0.047	7.932	−1.522	6.303	5.869	0.434	7.628	−1.325
53) JWH-207	5.796	6.065	−0.269	7.555	−1.759	5.429	5.806	−0.377	7.555	−2.126
54) JWH-208	6.747	6.740	0.007	7.198	−0.451	6.244	6.063	0.181	7.059	−0.815
55) JWH-209	6.127	6.343	−0.216	8.359	−2.232	5.869	5.998	−0.129	8.180	−2.311
56) JWH-237	7.420	7.597	−0.177	6.574	0.846	6.975	7.273	−0.298	7.026	−0.051
57) JWH-248*	5.988	6.152	−0.164	8.035	−2.047	6.182	6.471	−0.289	8.208	−2.026
58) JWH-249	8.075	7.839	0.236	6.238	1.837	7.699	7.453	0.246	6.933	0.766
59) JWH-250	7.958	7.845	0.113	7.849	0.109	7.481	7.217	0.264	8.294	−0.813
60) JWH-251	7.537	7.584	−0.047	5.041	2.496	6.836	7.239	−0.403	7.116	−0.280
61) JWH-252*	7.638	7.308	0.330	6.741	0.897	7.721	7.264	0.457	8.344	−0.623
62) JWH-253	7.207	6.996	0.211	6.350	0.857	7.076	6.916	0.160	8.279	−1.203
63) JWH-302	7.769	7.788	−0.019	7.547	0.222	7.051	7.110	−0.059	7.047	0.004
64) JWH-303	6.931	6.885	0.046	6.998	−0.067	6.860	7.031	−0.171	7.075	−0.215
65) JWH-305	7.823	7.915	−0.092	7.515	0.308	7.538	7.595	−0.057	7.317	0.221
66) JWH-306*	7.602	7.595	0.007	6.580	1.022	7.086	7.092	−0.006	6.638	0.448
67) JWH-311	7.638	7.687	−0.049	7.461	0.177	7.409	7.231	0.178	7.097	0.312
68) JWH-312*	7.142	7.184	−0.042	7.040	0.102	7.041	7.013	0.028	6.907	0.134
69) JWH-313	6.374	6.259	0.115	6.500	−0.126	6.438	6.375	0.063	6.468	−0.030
70) JWH-314	7.408	7.300	0.108	7.044	0.364	7.119	7.221	−0.102	7.032	0.087
71) JWH-315	6.366	6.798	−0.432	6.622	−0.256	6.740	7.006	−0.266	6.842	−0.102

[a] Observed binding affinity values
[b] Predicted binding affinity values in p*Ki* (p*Ki* = −log [*Ki*]) obtained by applying the CoMFA (steric/electrostatic) model.
[c] Predicted binding affinity values in p*Ki* (p*Ki* = −log [*Ki*]) obtained by applying the CoMSIA (hydrophobic) model.
[d] Difference between the observed versus CoMFA binding affinity values.
[e] Difference between the observed versus CoMSIA binding affinity values.
* Molecule from the test set.

Table 5
Statistical results for the best CoMFA and CoMSIA models of selectivity obtained for the training set and test set.

	q^2 [a]	N[b]	SEP[c]	r^2 [d]	SEE[e]	F[f]	r^2_{pred}[g]
CB1							
CoMFA std	0.649	7	0.055	0.853	0.035	39.932	0.839
CoMSIA steric + electrostatic	0.603	5	0.057	0.813	0.039	43.565	0.886
CoMSIA hydrophobic	0.597	6	0.058	0.822	0.039	37.802	0.431
CB2							
CoMFA std	0.645	6	0.063	0.814	0.046	35.703	0.870
CoMSIA steric + electrostatic	0.577	6	0.069	0.795	0.048	31.746	0.880
CoMSIA hydrophobic	0.567	8	0.072	0.798	0.049	23.266	0.490

[a] Cross-validation correlation coefficient.
[b] Number of components.
[c] Standard error of prediction.
[d] Correlation coefficient.
[e] Standard error of estimation.
[f] *F*-ratio.
[g] Correlation coefficient between the observed and predictive activities of the test set.

2.7. Statistical analysis of CoMFA and CoMSIA models

The statistical robustness of CoMFA and CoMSIA models was evaluated based on q^2, the cross-validated leave-one-out correlation coefficient. Models were considered to be robust when q^2 was greater than 0.5. Moreover, the standard deviation of the residuals of fit (SD_{res}) was calculated, in order to assess the predictive ability of the derived models. Compounds with residuals (s) greater than twice the standard deviation of the residuals have been considered as *outliers*, that is, compounds whose predicted activity was under- or overestimated by the model, considering the training set (internal predictivity) and the test set (external predictivity). As a whole, this methodology evaluates the robustness of the generated 3D-QSAR models and also gives deep insight into the full SAR of the compounds of this study.

3. Results and discussion

CoMFA and CoMSIA techniques were used to develop models for CB1 and CB2 receptor affinities and CB1/CB2 and CB2/CB1 receptor selectivities. The hypothetic bioactive conformer reported in the literature was used in this work [32,20]. Using the molecules of the training set, 3D-QSAR models were generated and validated with an external test set comprising 15 molecules (Table 1). CoMFA and CoMSIA 3D-QSAR models were derived for a set of 56 structurally related indole ligands of cannabinoid receptors by using alignment 1 due to lower values of RMS compared to alignment 2 (Fig. 3). A total of 12 models, 4 using CoMFA and 8 using CoMSIA were generated (Tables 3 and 5).

3.1. CoMFA studies using affinity data for CB1

The best CoMFA affinity model for CB1 ligands showed a q^2 value of 0.785 with a number of the optimal components equal to 6 and a combination of cutoff values of 25 and 35 kcal mol^{-1} for the steric and electrostatic field contributions, respectively. A non-cross-validated r^2 of 0.926 with F of 102.532 was also observed with this model. Table 3 shows PLS statistics of the best CoMFA affinity model for CB1.

3.1.1. Visual inspection of 3D contour maps generated by CoMFA with affinity data for CB1 receptors

CoMFA steric and electrostatic fields for CB1 affinity based on PLS analysis were represented as 3D contour plots in Fig. 4a and b, using compounds with the highest and lowest affinities of the training set, JWH-210 (**27**, in purple) and JWH-265 (**43**), respectively, as reference structures (Table 1). The steric contour map shows a green region (sterically favored) surrounding both the ethyl group present in the R_4 position of the naphthyl ring and the *n*-pentyl substituent attached to the indole nitrogen of JWH-210 (**27**). Inversely, compound JWH-265 (**43**) presents an unfavorable interaction of the methoxy group in the R_3 position of the naphthyl ring, lying in a sterically forbidden yellow region of the contour map. Besides, JWH-265 (**43**) does not show any favorable interactions with the substituent at the R_1 position of the indole ring, which further explains the low affinity of this compound (Fig. 4a).

The visual inspection of the steric contour maps of the best CoMFA affinity model (Fig. 4a) towards CB1 reveals that compounds that bear hydrogen in the R_4 position of the naphthyl ring, an *n*-propyl chain instead of *n*-pentyl in the R_1 position and a methyl in the R_2 position of the indole ring tend to have reduced binding affinity for CB1. These data suggest that the substitution pattern in those positions of the molecular skeleton is very important for optimization of interactions with receptor CB1. This can be better exemplified when we compare compounds JWH-072 (**6**, $pKi_{CB1} = 5.978$) and JWH-018 (**3**, $pKi_{CB1} = 8.045$) that bear an *n*-propyl and an *n*-pentyl group in the R_1 position of the indole ring, respectively. In the latter case, the addition of two methylene groups, transforming the propyl chain in pentyl, promotes

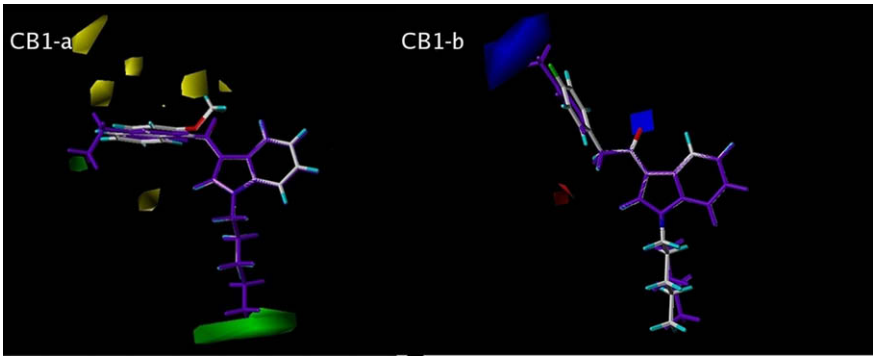

Fig. 4. Steric (a) and electrostatic (b) contour maps of the best CoMFA affinity model for CB1 receptors are represented by compounds with the highest p*Ki* value, JWH-210 (in purple) and the lowest p*Ki* value, JWH-265 superposed in the steric contour plot, and the compounds JWH-208 (in purple) and JWH-313, respectively, superposed in the electrostatic contour plot. Steric contour plots: green contours (80% contribution) indicate regions where an increase in steric bulk will enhance affinity, whereas yellow contours (20% contribution) indicate sterically disfavored regions. Electrostatic contour plots: blue contours (80% contribution) and red contours (20% contribution) correspond to regions where an increase in positive or negative charge, respectively, is favorable for binding properties. (For interpretation of the references to colour in this figure legend, the reader is referred to the web version of this article.)

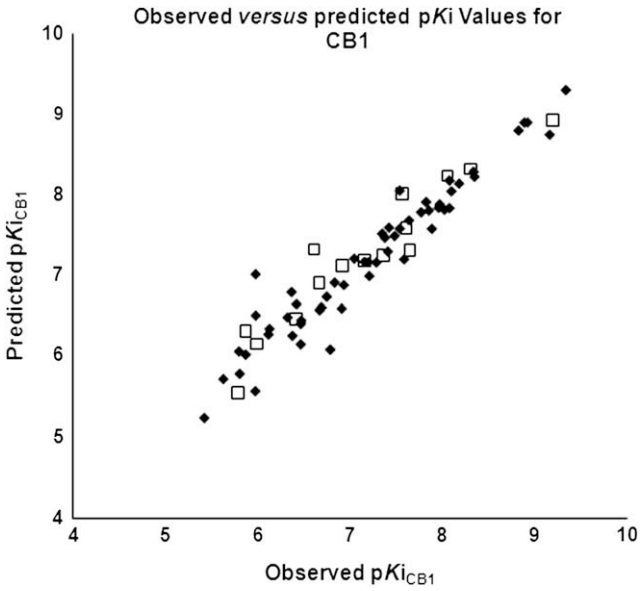

Fig. 5. Plot of predicted *versus* observed p*K*i values derived from the steric/electrostatic CoMFA affinity model of the training (in black) and test (in white) sets of CB1 ligands.

a difference in binding affinity of 116-fold (*K*i values), confirming the pharmacophoric importance of these substituents for molecular recognition by the target CB1 receptor.

Additionally, ligands that present an *n*-pentyl chain in the R_1 position along with $-CH_3$, $-C_2H_5$, $-C_3H_7$, $-OCH_3$ and $-OC_2H_5$ in the R_4 position of the naphthyl ring, *e.g.* JWH-122 (**13**, pKi_{CB1} = 9.161), JWH-149 (**15**, pKi_{CB1} = 8.301), JWH-210 (**27**, pKi_{CB1} = 9.337), JWH-213 (**30**, pKi_{CB1} = 8.823), JWH-182 (**25**, pKi_{CB1} = 9.187), JWH-181 (**24**, pKi_{CB1} = 8.886), JWH-081 (**9**, pKi_{CB1} = 8.920), JWH-098 (**11**, pKi_{CB1} = 8.346), JWH-258 (**38**, pKi_{CB1} = 8.337) and JWH-260 (**40**, pKi_{CB1} = 7.537) are part of a group of compounds that have the highest affinity values for CB1. Among them, compounds JWH-260 (**40**), JWH-098 (**11**), JWH-181 (**24**), JWH-213 (**30**) and JWH-149 (**15**), which presented a methyl group in the R_2 position of the indole ring, have demonstrated good affinity values for the CB1 receptor, in spite to be frequently associated with decreasing receptor binding affinity. However, structure–activity analysis of these derivatives suggests that substitution in R_4 and R_1 positions of the naphthyl and the indole ring, respectively, represents the most important pharmacophoric subunits, justifying the good binding profile of these compounds.

We may hypothesize that, in some compounds, the methyl group attached to the R_2 position of the indole ring would lead to a conformational change of the vicinal naphthyl ring, adequately orientating the side chains and improving molecular recognition within the CB1 receptor. This behavior could be evidenced through the comparison of the binding affinity profile of ligands that also bear an *n*-propyl chain in the R_1 position of the indole ring, *e.g.* JWH-072 (**6**, pKi_{CB1} = 5.978) and JWH-015 (**2**, pKi_{CB1} = 6.785). Besides, *para*-substituted (X_3) analogues from benzylcarbonyl series show a decreased affinity for CB1 receptor when compared to substitutions in other positions (X_1 and X_2). This deleterious effect is emphasized when the ligand also has a methyl group in the R_2 position of the indole ring, *e.g.* compounds JWH-209 (**55**, pKi_{CB1} = 6.127), JWH-202 (**48**, pKi_{CB1} = 5.775) and JWH-207 (**53**, pKi_{CB1} = 5.796).

Visual inspection of the CoMFA steric contour map (Fig. 4a) shows that groups in the X_3 position lie in a yellow field, which does not favor large substituents (bigger than hydrogen). Additionally, in the analysis of the CoMFA electrostatic contour map (Fig. 4b), these groups also lie in a blue field, which is unfavorable for the presence of electron-rich groups, such as *p*-F, *p*-Cl, *p*-Br and *p*-OCH_3. These observations justify the low p*K*i values for the binding at CB1 receptor subtype through the comparison of the compounds JWH-208 (**54**, pKi_{CB1} = 6.747, in purple) and JWH-313 (**69**, pKi_{CB1} = 6.374). In the CoMFA electrostatic model, compound JWH-208 (**54**) presents a greater affinity for the CB1 receptor, when compared to the ligand with the p*K*i value demonstrated by the compound JWH-313 (**69**). This may be explained by the presence of an electron-rich group in the X_3 position of the benzylcarbonyl subunit of JWH-313 (**69**) which decreases its affinity for CB1 in comparison with compound JWH-208 (**54**) that bears a methyl group in the corresponding position.

The predicted p*K*i values for the compounds exploited in our database using the CoMFA affinity model for CB1 receptors are given in Table 4. Fig. 5 shows the plot of observed *versus* predicted p*K*i values obtained from the best CoMFA affinity model for CB1, highlighting the training and the test sets.

3.2. CoMFA studies using affinity data for CB2

The best CoMFA affinity model obtained for indole ligands of CB2 receptors showed a good q^2 of 0.751 using 6 components. A non-cross-validated r^2 of 0.898 with an *F* value of 71.707 was also observed with this model (Table 3).

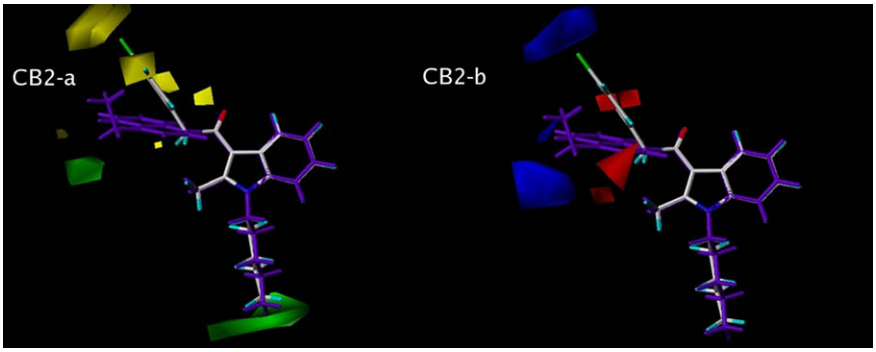

Fig. 6. Steric (a) and electrostatic (b) contour maps of the best CoMFA affinity model for CB2 receptor ligands. Compounds JWH-213 (in purple) and JWH-207 are shown inside the fields. Steric contour plots: green contours (80% contribution) indicate regions where an increase in steric bulk will enhance affinity, whereas yellow contours (20% contribution) indicate sterically disfavored regions. Electrostatic contour plots: blue contours (80% contribution) and red contours (20% contribution) correspond to regions where an increase in positive or negative charge, respectively, is favorable for binding properties. (For interpretation of the references to colour in this figure legend, the reader is referred to the web version of this article.)

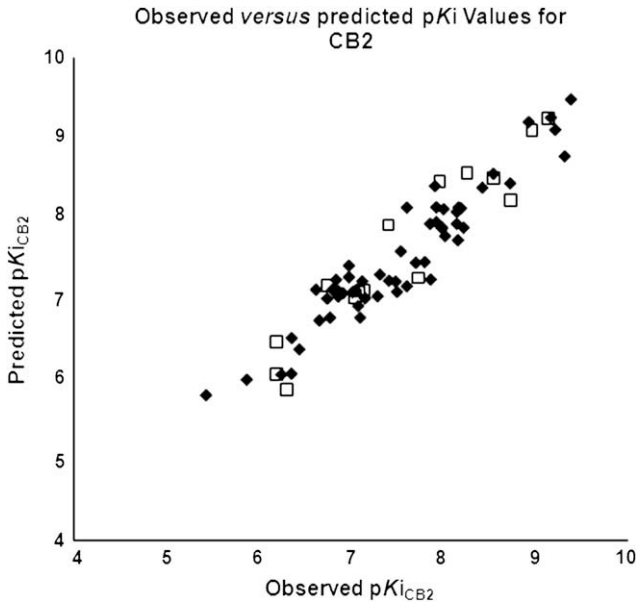

Fig. 7. Observed *versus* predicted p*K*i values derived from the steric/electrostatic CoMFA affinity model of the training (in black) and test (in white) sets of CB2 ligands.

3.2.1. *Visual inspection of 3D contour maps generated by CoMFA with affinity data for CB2 receptors*

The CoMFA steric and electrostatic contour maps of the developed affinity model towards CB2 receptors are depicted in Fig. 6a and b with the compounds JWH-213 (**30**, p$Ki_{CB2} = 9.377$, in purple) and JWH-207 (**53**, p$Ki_{CB2} = 5.429$) as reference structures (Table 1). Compound JWH-213 (**30**) is the molecule within the database that shows the highest affinity for CB2 receptors and this profile could be justified by favorable interactions demonstrated in the CoMFA steric map, where the ethyl group in R_4 position of the naphthyl ring and the *n*-pentyl chain attached to the indolic nitrogen (R_1) show favorable interactions in green fields of the model (Fig. 6a).

Moreover, the visual inspection of compound JWH-207 (**53**), which has the lowest affinity for CB2 among the compounds of our database (Table 1), shows the chlorine substituent in the X_3 position of the benzylcarbonyl subunit and the aromatic ring itself in a position close to a yellow field of the steric contour map, unfavorable for the binding affinity at CB2 receptors (Fig. 6a). Additionally, the chlorine atom of JWH-207 (**53**) is also close to a blue field in the CoMFA electrostatic contour map, which is unfavorable for electron-rich substituents (Fig. 6b).

The visual inspection of the CoMFA steric contour map obtained for CB2 receptor ligands shows that, contrary to the contour map obtained for CB1 receptors (Fig. 4a), substitution in the R_2 position of the indole ring by a methyl group does not influence binding affinity as much as it does upon binding to CB1. This is corroborated by the lack of steric contour maps around the methyl group at R_2 position in the model obtained for CB2 (Fig. 6a). This fact is supported by the comparison between JWH-164 (**20**, p$Ki_{CB2} = 8.161$) and JWH-159 (**17**, p$Ki_{CB2} = 7.982$), which bear a hydrogen and a methyl group in R_2 position of the indole ring, respectively, since the difference in binding affinity between them is only 0.179, while the difference in p*K*i for CB1 is 0.261 (Table 2).

The CoMFA electrostatic contour map for ligands of CB2 receptors (Fig. 6b) has demonstrated few favorable regions for interaction with electron-rich groups (red contour map), as it has been observed in the model for CB1 receptors. This result is expected, since docking studies with homology models of both CB1 and CB2 receptors have shown that the active site is mostly composed of hydrophobic amino acid residues that interact through aromatic stacking [11,20].

Other similarities with the model that has been built for CB1 are the presence of two sterically favored regions (green) around substituents in the R_4 and R_1 positions of the naphthyl and indole rings, respectively. An additional unfavorable (yellow) steric contour map around the X_3 position of the benzylcarbonyl subunit characterizes itself as affinity-decreasing for both CB1 (Fig. 4a) and CB2 (Fig. 6a) receptors. Also, the analogues in which the secondary aryl ring is *ortho* substituted (X_1 position) have shown highest affinity for both CB1 and CB2, as exemplified by compounds JWH-250 (**59**, p$Ki_{CB1} = 7.958$ and p$Ki_{CB2} = 7.481$), JWH-306 (**66**, p$Ki_{CB1} = 7.602$ and p$Ki_{CB2} = 7.086$), JWH-251 (**60**, p$Ki_{CB1} = 7.537$ and p$Ki_{CB2} = 6.836$), JWH-252 (**61** p$Ki_{CB1} = 7.638$ and p$Ki_{CB2} = 7.721$), JWH-203 (**49**, p$Ki_{CB1} = 8.096$ and p$Ki_{CB2} = 8.155$), JWH-204 (**50**, p$Ki_{CB1} = 7.886$ and p$Ki_{CB2} = 7.602$), JWH-249 (**58**, p$Ki_{CB1} = 8.075$ and p$Ki_{CB2} = 7.699$), JWH-305 (**65**, p$Ki_{CB1} = 7.823$ and p$Ki_{CB2} = 7.538$), which can be explained through the visual inspection of the CoMFA steric contour maps that lack unfavorable (yellow) fields (Fig. 6a). The same is not true for the analogues presenting substituents at X_2 and X_3 positions, *e.g.* compounds JWH-208 (**54**, p$Ki_{CB1} = 6.747$ and p$Ki_{CB2} = 6.244$), JWH-209 (**55**, p$Ki_{CB1} = 6.127$ and p$Ki_{CB2} = 5.869$), JWH-312 (**68**, p$Ki_{CB1} = 7.142$ and p$Ki_{CB2} = 7.041$), JWH-315 (**71**, p$Ki_{CB1} = 6.366$ and p$Ki_{CB2} = 6.740$), JWH-313 (**69**, p$Ki_{CB1} = 6.374$ and p$Ki_{CB2} = 6.438$).

The predicted activities using the CoMFA affinity model for CB2 are given in Table 4 and Fig. 7 shows the plot of observed *versus* predicted p*K*i for the training set and the test set obtained through quantitative analysis of the model.

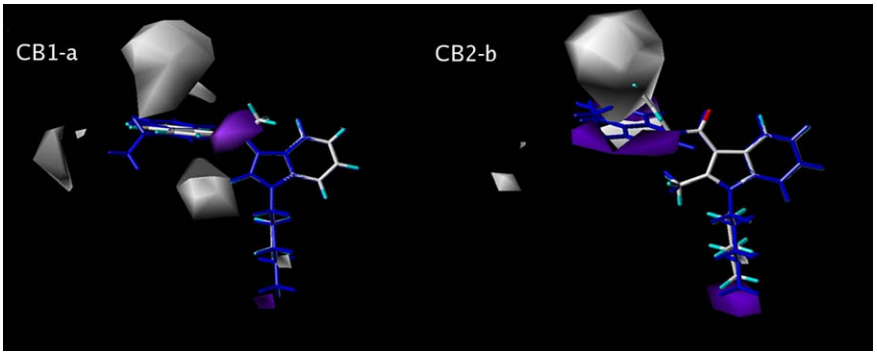

Fig. 8. CoMSIA hydrophobic contour maps for the affinity of indole ligands to CB1 (a) and CB2 (b) receptors. Compounds JWH-210 (in blue)/JWH-265 and JWH-213 (in blue)/JWH-207 are shown inside the fields of the models (a) and (b), respectively. Purple regions (80% contribution) indicate areas where hydrophobic groups increase activity and white regions (20% contribution) indicate areas where hydrophobic groups decrease activity. (For interpretation of the references to colour in this figure legend, the reader is referred to the web version of this article.)

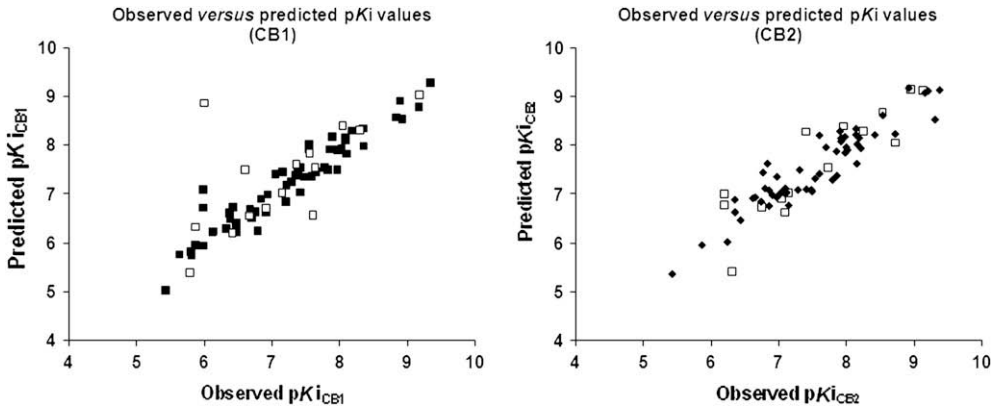

Fig. 9. Observed *versus* predicted p*K*i values derived from the CoMSIA hydrophobic affinity model of the training (in black) and test (in white) sets of CB1 and CB2 ligands.

3.3. CoMSIA studies using affinity data for CB1 and CB2

To enhance the assessment made by CoMFA steric and electrostatic contour maps, we built models with the same properties previously evaluated as well as hydrophobic, hydrogen bonding acceptor and donor properties, using CoMSIA method. The CoMSIA steric and electrostatic models corroborated the results previously obtained by CoMFA, which represent a positive result in the validation of the developed 3D-QSAR models. The best affinity models for CB1 and CB2 receptors generated q^2 values of 0.743 and 0.759, respectively. Also, the models showed non-cross-validated r^2 values of 0.908 and 0.879 and *F* values of 67.681 and 59.199, respectively (Table 3).

The visual inspection, along with the statistics of the hydrogen bonding contour maps revealed that this property did not generate good models, as expected from the previous bad performance of the electrostatic contour maps (data not labeled). Thus, this property has been discarded from our structure–activity relationship (SAR) studies. However, the great advantage of CoMSIA in our study was the construction of hydrophobic contour maps which have shown to be highly correlated to the steric contour maps created by CoMFA and have proven to be an excellent tool used in our SAR analysis. This result was expected due to the mainly hydrophobic nature of the interactions of cannabinoid ligands with the receptors [40].

The predicted activities using the CoMSIA steric/electrostatic models of affinities towards CB1 receptors, and the residue values of the training and the test sets as well as the plot of observed *versus* predicted p*K*i for the training and the test were very similar to those obtained by CoMFA. The CoMSIA hydrophobic contour maps of affinity showed q^2 values of 0.716 and 0.713 for CB1 and CB2, respectively (Table 3). Besides, consistent r^2 values of the non-cross-validation equal to 0.907 and 0.868 with low values of standard error of estimate (SEE) below 0.330 for both and Fischer test values of 57.230 and 65.998 for CB1 and CB2 affinities, respectively, have been obtained (Table 3).

The CoMSIA hydrophobic contour maps of affinity for cannabinoid CB1 and CB2 receptors are depicted in Fig. 8, demonstrating compounds JWH-210 (**27**, in blue) and JWH-265 (**43**) inside the map (a) and JWH-207 (**53**) and JWH-213 (**30**, in blue) inside the map (b), respectively. In the CB1 model (Fig. 8a), there is a lack of unfavorable interactions made by the ligand with the highest affinity of our database. In addition, compound JWH-210 (**27**) also has its *n*-pentyl chain in a region that allows the presence of hydrophobic groups. However, two unfavorable interactions have been observed with compound JWH-265 (**43**). One of them is caused by the oxygen atom of the methoxy group in the R_3 position of the naphthyl ring in a region favorable to the presence of hydrophobic groups and the other involves the *n*-propyl chain at R_1 position that lies close to a contour map unfavorable to the presence of hydrophobic groups. These data justify its lower affinity in comparison to compound JWH-210 (**27**) (Table 1).

The analysis of the hydrophobic contour maps of the best affinity model towards CB2 receptor (Fig. 8b) showed that the ligand with the highest affinity, JWH-213 (**30**, in blue), does not have any unfavorable interaction with the maps, and yet shows the ethyl group in the R_4 position of the naphthyl ring close to the region that is favorable to the presence of hydrophobic groups, in opposition to what was observed for compound JWH-207 (**53**), that despite having a *para*-Cl substituent lying close to an unfavorable hydrophobic field (gray, Fig. 8b), had its p*K*i value overestimated by the model in 2.16 logarithmic units. This result may be due to the proximity of the *n*-pentyl chain in the R_1 position to a region that is favorable to the interaction with hydrophobic groups, which seems to be statistically more significant to the affinity for CB2 receptors (Fig. 8b).

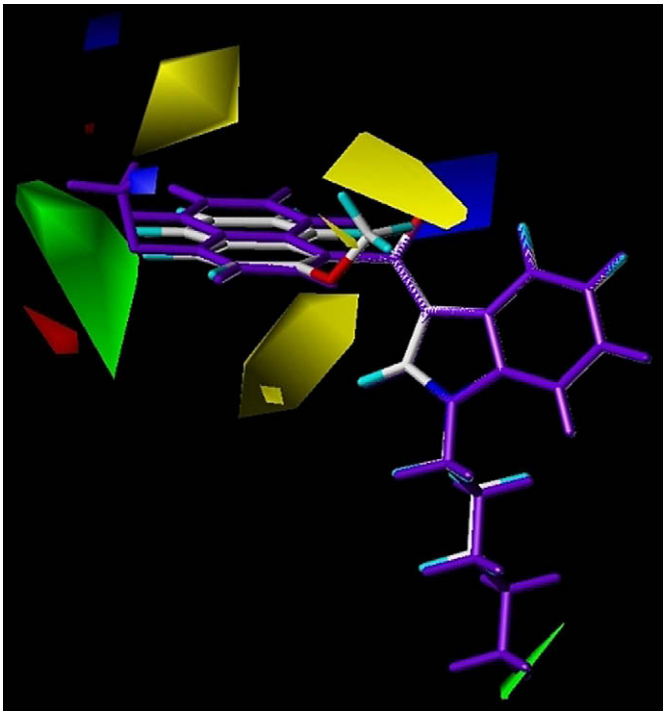

Fig. 10. Steric and electrostatic contour maps from the best CoMFA model of selectivity towards CB1 receptors. Compounds JWH-081 (in purple) and JWH-265 are shown inside the fields. (For interpretation of the references to colour in this figure legend, the reader is referred to the web version of this article.)

Table 6
Observed and predicted binding selectivity values, given in p*Ki* (p*Ki* = −log [*Ki*]) obtained by applying the CoMFA (steric/electrostatic) and CoMSIA (hydrophobic) models for cannabinoid CB1 and CB2 receptor ligands and the difference between the observed versus CoMFA and CoMSIA predicted selectivity values towards CB1 and CB2 receptors.

Compound	[a]CB1	[b]CB1	[d]CB1	[c]CB1	[e]CB1	[a]CB2	[b]CB2	[d]CB2	[c]CB2	[e]CB2
1) JWH-007	0.939	0.907	0.032	0.920	0.019	1.064	1.115	−0.051	1.093	−0.029
2) JWH-015	0.863	0.845	0.018	0.851	0.012	1.158	1.181	−0.023	1.174	−0.016
3) JWH-018*	0.942	0.961	−0.019	0.969	−0.027	1.061	1.062	−0.001	1.037	0.024
4) JWH-046	0.829	0.853	−0.024	0.848	−0.019	1.205	1.167	0.038	1.166	0.039
5) JWH-048	0.856	0.915	−0.059	0.917	−0.061	1.168	1.101	0.067	1.085	0.083
6) JWH-072	0.883	0.899	−0.016	0.900	−0.017	1.132	1.128	0.004	1.119	0.013
7) JWH-076	0.956	0.906	0.050	0.897	0.059	1.045	1.115	−0.070	1.111	−0.066
8) JWH-079	0.960	1.008	−0.048	0.977	−0.017	1.040	1.008	0.032	1.029	0.011
9) JWH-081	1.128	1.070	0.058	1.046	0.082	0.886	0.942	−0.056	0.948	−0.062
10) JWH-094	0.901	0.903	−0.002	0.910	−0.009	1.109	1.097	0.012	1.104	0.005
11) JWH-098	0.957	0.965	−0.008	0.979	−0.022	1.044	1.032	0.012	1.022	0.022
12) JWH-120	0.727	0.885	−0.158	0.881	−0.154	1.374	1.140	0.234	1.147	0.227
13) JWH-122	1.026	0.947	0.079	0.950	0.076	0.973	1.074	−0.101	1.066	−0.093
14) JWH-148	0.879	0.832	0.047	0.833	0.046	1.136	1.193	−0.057	1.202	−0.066
15) JWH-149*	0.908	0.894	0.014	0.901	0.007	1.100	1.127	−0.027	1.121	−0.021
16) JWH-153*	0.829	0.853	−0.024	0.917	−0.088	1.205	1.190	0.015	1.110	0.095
17) JWH-159	0.920	0.950	−0.030	0.964	−0.044	1.086	1.065	0.021	1.051	0.035
18) JWH-160	0.913	0.889	0.024	0.898	0.015	1.094	1.130	−0.036	1.129	−0.035
19) JWH-163	0.820	0.809	0.011	0.874	−0.054	1.219	1.224	−0.005	1.174	0.045
20) JWH-164	1.002	1.006	−0.004	1.013	−0.011	0.997	0.997	0.000	0.990	0.007
21) JWH-165	0.935	0.940	−0.005	0.936	−0.001	1.068	1.067	0.001	1.083	−0.015
22) JWH-166*	0.843	0.874	−0.031	0.956	−0.113	1.185	1.153	0.032	1.074	0.111
23) JWH-180	0.946	0.932	0.014	0.944	0.002	1.057	1.075	−0.018	1.059	−0.002
24) JWH-181	0.965	0.973	−0.008	0.986	−0.021	1.036	1.008	0.028	0.999	0.037
25) JWH-182*	1.025	0.994	0.031	1.012	0.013	0.975	1.009	−0.034	0.977	−0.002
26) JWH-189	0.919	0.899	0.020	0.914	0.005	1.087	1.089	−0.002	1.102	−0.015
27) JWH-210	1.019	1.017	0.002	0.982	0.037	0.981	0.971	0.010	1.007	−0.026
28) JWH-211	0.903	0.896	0.007	0.904	−0.001	1.107	1.109	−0.002	1.084	0.023
29) JWH-212	0.935	0.935	0.000	0.912	0.023	1.069	1.078	−0.009	1.101	−0.032
30) JWH-213	0.941	0.943	−0.002	0.932	0.009	1.062	1.065	−0.003	1.075	−0.013
31) JWH-234	0.959	0.975	−0.016	0.975	−0.016	1.042	1.038	0.004	1.016	0.026
32) JWH-235	0.936	0.913	0.023	0.907	0.029	1.067	1.103	−0.036	1.097	−0.030
33) JWH-236	0.886	0.860	0.026	0.858	0.028	1.127	1.155	−0.028	1.152	−0.025
34) JWH-239	0.887	0.892	−0.005	0.873	0.014	1.126	1.109	0.017	1.147	−0.021
35) JWH-240	0.964	0.953	0.011	0.965	−0.001	1.036	1.054	−0.018	1.047	−0.011
36) JWH-241	0.934	0.919	0.015	0.908	0.026	1.069	1.076	−0.007	1.097	−0.028
37) JWH-242	0.901	0.906	−0.005	0.921	−0.020	1.109	1.099	0.010	1.097	0.012
38) JWH-258	1.044	1.048	−0.004	1.039	0.005	0.957	0.956	0.001	0.963	−0.006
39) JWH-259*	0.933	0.984	−0.051	0.918	0.015	1.071	1.005	0.066	1.104	−0.033
40) JWH-260	0.991	1.000	−0.009	1.010	−0.019	1.008	0.994	0.014	0.984	0.024
41) JWH-261	0.918	0.919	−0.001	0.929	−0.011	1.088	1.067	0.021	1.077	0.011
42) JWH-262	0.915	0.939	−0.024	0.943	−0.028	1.092	1.071	0.021	1.054	0.038
43) JWH-265	0.763	0.749	0.014	0.731	0.032	1.309	1.318	−0.009	1.329	−0.020
44) JWH-267	0.788	0.818	−0.030	0.807	−0.019	1.268	1.254	0.014	1.240	0.028
45) JWH-268*	0.792	0.779	0.013	0.764	0.028	1.262	1.295	−0.033	1.289	−0.027
46) JWH-167	1.072	1.025	0.047	1.079	−0.007	0.964	0.971	−0.007	0.919	0.045
47) JWH-201	0.928	0.923	0.005	0.924	0.004	1.063	1.065	−0.002	1.097	−0.034
48) JWH-202*	0.879	0.917	−0.038	0.878	0.001	1.071	1.067	0.004	1.150	−0.079
49) JWH-203	1.035	1.024	0.011	1.034	0.001	1.007	0.959	0.048	0.966	0.041
50) JWH-204	1.061	1.038	0.023	1.053	0.008	0.963	0.964	−0.001	0.944	0.019
51) JWH-205*	1.010	0.998	0.012	1.012	−0.002	0.976	0.996	−0.020	0.993	−0.017
52) JWH-206*	1.088	1.073	0.015	1.082	0.006	0.983	0.923	0.060	0.891	0.092
53) JWH-207	1.044	1.040	0.004	1.039	0.005	0.936	0.961	−0.025	0.940	−0.004
54) JWH-208	1.075	1.087	−0.012	1.069	0.006	0.925	0.913	0.012	0.918	0.007
55) JWH-209	1.031	1.054	−0.023	1.026	0.005	0.957	0.950	0.007	0.967	−0.010
56) JWH-237	1.069	1.051	0.018	1.066	0.003	0.939	0.960	−0.021	0.923	0.016
57) JWH-248*	1.239	0.965	0.274	1.235	0.004	1.032	1.051	−0.019	0.769	0.263
58) JWH-249	1.042	1.056	−0.014	1.048	−0.006	0.953	0.945	0.008	0.947	0.006
59) JWH-250	1.087	1.065	0.022	1.093	−0.006	0.940	0.942	−0.002	0.928	0.012
60' JWH-251	1.060	1.080	−0.020	1.062	−0.002	0.906	0.931	−0.025	0.954	−0.048
61) JWH-252*	1.018	1.043	−0.025	1.020	−0.002	1.010	0.958	0.052	1.003	0.007
62) JWH-253	1.032	1.009	0.023	1.037	−0.005	0.981	0.974	0.007	0.978	0.003
63) JWH-302	1.074	1.105	−0.031	1.074	0.000	0.907	0.901	0.006	0.935	−0.028
64) JWH-303	0.994	1.004	−0.010	0.993	0.001	0.989	1.003	−0.014	1.008	−0.019
65) JWH-305	0.998	1.048	−0.050	1.005	−0.007	0.963	0.947	0.016	0.974	−0.011
66) JWH-306*	1.015	1.023	−0.008	1.020	−0.005	0.932	0.979	−0.047	0.995	−0.063
67) JWH-311	1.040	1.033	0.007	1.035	0.005	0.969	0.972	−0.003	0.969	0.000
68) JWH-312*	1.025	1.025	0.000	1.023	0.002	0.985	0.973	0.012	0.976	0.009
69) JWH-313	1.011	1.004	0.007	1.010	0.001	1.009	0.991	0.018	0.986	0.023
70) JWH-314	0.994	0.996	−0.002	0.990	0.004	0.960	1.011	−0.051	1.020	−0.060
71) JWH-315	0.978	0.988	−0.010	0.979	−0.001	1.058	1.012	0.046	1.026	0.032

[a] Observed binding selectivity values.
[b] Predicted selectivity values in p*Ki* (p*Ki* = −log [*Ki*]) obtained by applying the CoMFA (steric/electrostatic) model.
[c] Predicted selectivity values in p*Ki* (p*Ki* = −log [*Ki*]) obtained by applying the CoMSIA (hydrophobic) model.
[d] Difference between the observed versus CoMFA binding selectivity values.
[e] Difference between the observed versus CoMSIA binding selectivity values.
* Molecule from the test set.

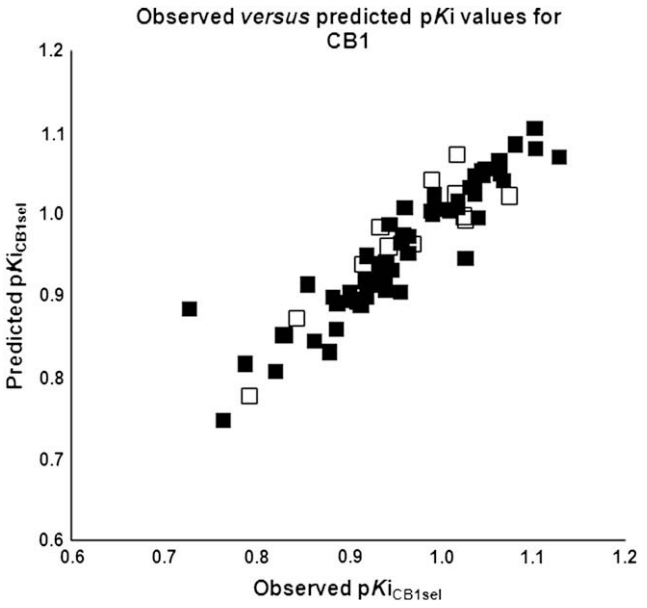

Fig. 11. Plots of observed *versus* predicted p*K*i values for the selectivity model towards CB1 for ligands used as training (in black) and test (in white) sets.

In short, the inspection of the CoMSIA hydrophobic contour built for CB1 ligands reveals the presence of an unfavorable field (gray) (Fig. 8a) surrounding the R_2 position of the indole ring, in agreement with results previously discussed from CoMFA steric model. In the hydrophobic model for CB2 ligands, there were no fields around the R_2 position (Fig. 8b), suggesting that the introduction of substituents at this point is not important for the affinity of the studied indole ligands to CB2 receptors. Nevertheless, as already demonstrated by the CoMSIA hydrophobic model obtained for CB1, the substitution of the X_3 position in the secondary aryl subunit is unfavorable for hydrophobic substituents such as Cl, Br and CH_3. The predicted activities using the CoMSIA hydrophobic model of affinity for CB2 are given in Table 4 and Fig. 9 shows the plot of observed *versus* predicted p*K*i values for the training and the test sets.

3.4. CoMFA and CoMSIA studies using CB1 and CB2 selectivity data

Selectivity towards a specific bioreceptor is fundamental to assure that a determined bioactive substance could present minimized side effects resultant from the bind to two or more distinct therapeutic targets as the cannabinoid CB1 and CB2 receptors. Keeping that in mind, we built 3D-QSAR models of selectivity to CB1 and CB2 using CoMFA and CoMSIA methods, mapping steric, electrostatic and hydrophobic properties with the goal of achieving a structure–activity relationship of selectivity within the database of indole ligands.

First, we used the CoMFA methodology in the construction of steric/electrostatic models of selectivity for both subtypes of receptors. Since the least selective molecule for CB1, JWH-120 (**12**, $pKi_{CB1sel} = 0.728$) has proven to be an *outlier* for failing to show a structure–activity relationship with the database used in the study of 3D-QSAR, it has been left out of the visual inspection and the contour maps of the best CoMFA model generated with selectivity data for CB1 surround the second least CB1-selective molecule JWH-265 (**43**, $pKi_{CB1sel} = 0.764$) and the most selective molecule of the data set for CB1, JWH-081 (**9**, $pKi_{CB1sel} = 1.128$, in purple), displayed in Fig. 10. Compound JWH-081 (**9**) showed favorable interactions in the both steric and electrostatic fields, involving the ethyl group in the R_4 position of the naphthyl ring and the *n*-pentyl group connected to the indole ring.

Unlike the previously mentioned ligand, JWH-081 (**9**), compound JWH-265 (**43**) lacks favorable interactions and makes an additional unfavorable interaction through the methoxy group present in the R_3 position of the naphthyl ring (Fig. 10). This result corroborates the difference in selectivity observed between both ligands, with a CB1/CB2 p*K*i ratio equal to 0.364 (Table 1). Moreover, the visual inspection of the CoMFA/CoMSIA steric and CoMSIA hydrophobic models built for CB1 and CB2 ligands has revealed an unfavorable field around the R_2 position of the indole ring in the CB1 affinity model that is not present in the model of affinity towards CB2. Thus, 3D-QSAR studies have shown that the introduction of substituents in that position would decrease affinity to CB1 receptors. Differently, it has no importance for the affinity of indole ligands to CB2 receptors. Compounds JWH-149 (**15**, $pKi_{CB1/CB2\ ratio} = 0.909$), JWH-148 (**14**, $pKi_{CB1/CB2\ ratio} = 0.880$), JWH-211 (**28**, $pKi_{CB1/CB2\ ratio} = 0.903$), JWH-213 (**30**, $pKi_{CB1/CB2\ ratio} = 0.941$), JWH-189 (**26**, $pKi_{CB1/CB2\ ratio} = 0.919$), JWH-241 (**36**, $pKi_{CB1/CB2\ ratio} = 0.935$), JWH-046 (**4**, $pKi_{CB1/CB2\ ratio} = 0.829$), JWH-236 (**33**, $pKi_{CB1/CB2\ ratio} = 0.887$), JWH-268 (**45**, $pKi_{CB1/CB2\ ratio} = 0.792$) and JWH-094 (**10**, $pKi_{CB1/CB2\ ratio} = 0.901$) are the examples of indole derivatives that bear a methyl group in the above mentioned position which, as predicted by the models, have demonstrated a higher affinity towards CB2 in comparison to CB1. Nevertheless, this is only true with analogues that have naphthyl and not more flexible aryl rings bound to the indole nucleus.

We may hypothesize that this effect is due to a larger steric repulsion between the naphthyl ring and the methyl group at R_2, leading to a secondary bioactive conformation that is more favorable for recognition by amino acid residues in CB2 than CB1 receptors. Since the side chain with other simplified aryl rings is

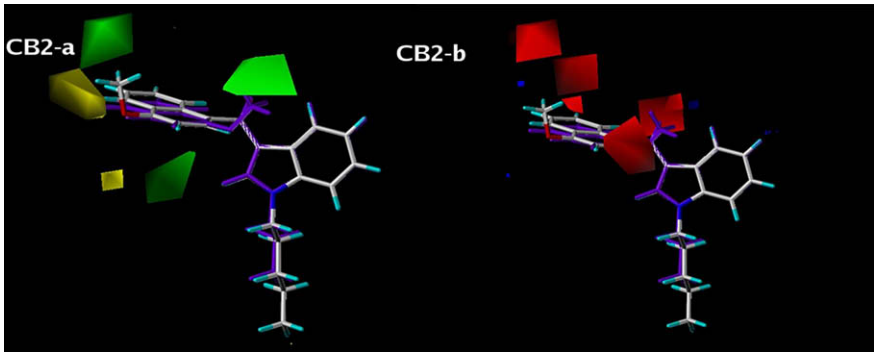

Fig. 12. Steric (a) and electrostatic (b) contour maps from the best CoMFA selectivity model towards CB2 receptors. Compounds JWH-265 (in purple) and JWH-081 are shown inside the fields. (For interpretation of the references to colour in this figure legend, the reader is referred to the web version of this article.)

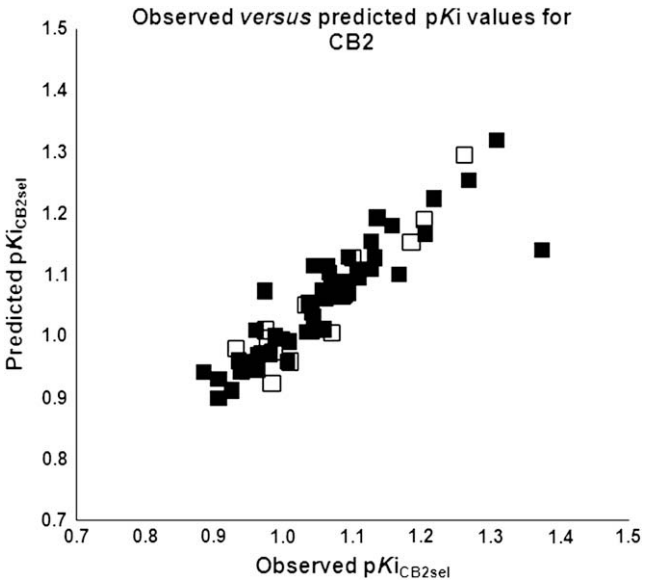

Fig. 13. Plots of observed *versus* predicted p*K*i values for the model of selectivity towards CB2 for ligands used as training (in black) and test (in white) sets.

more flexible, the referred bioactive conformation may not be so favored at the target bioreceptor.

The selectivity model for CB1 showed significant statistical values (Table 5), in addition to demonstrating good correlation to the experimental selectivity obtained using CB1/CB2 p*K*i ratio. The observed *versus* predicted selectivity values are shown in Table 6 and Fig. 11 shows the plot of observed *versus* predicted p*K*i for the training set and the test set obtained through quantitative analysis of the model.

Aiming to correlate and validate the models of selectivity built using the CB1/CB2 p*K*i ratio; we also built models inverting the CB2/CB1 p*K*i ratio, with the goal of checking if there was a qualitative reversal of the steric and electrostatic contour maps. In this process, we used the same molecules employed in the model above. However, this time the second molecule of greater selectivity was JWH-265 (**43**, in purple) and lowest was JWH-081 (**9**). Compound JWH-265 (**43**) showed favorable interactions in the both steric (Fig. 12a) and electrostatic (Fig. 12b) maps with the methoxy group in the R_3 position of the naphthyl ring. Moreover, it did not occupy unfavorable regions in the maps, unlike compound JWH-081 (**9**) that has the methoxy group in the R_4 position of the naphthyl ring in an unfavorable region, decreasing its selectivity.

The comparison between selectivity models for CB1/CB2 and CB2/CB1 has provided a qualitative analysis through the visual inspection of the contour maps that revealed inverted fields (Fig. 12a and b). That is, in the best CoMFA model for CB1 the presence of bulky substituents in the R_3 position of the naphthyl and flexible aryl rings showed to be unfavorable and the same region turns out to be favorable for naphthyl substitution in the best CoMFA model for CB2. Therefore, this molecular region is a probable pharmacophore and may be modified through the introduction of other different groups aiming at achieving selectivity towards CB2.

This has been observed experimentally with compounds JWH-265 (**43**, $pKi_{CB2/CB1\ ratio} = 1.309$) and JWH-268 (**45**, $pKi_{CB2/CB1\ ratio} = 1.262$), which are significantly selective towards CB2 (Table 6). Additionally, the analysis of the CoMFA/CoMSIA electrostatic and CoMSIA hydrophobic models for CB1 ligand affinity shows few regions that are favorable to the introduction of electron-rich groups. However, the electrostatic contour map of selectivity for CB2 shows red fields surrounding the X_3 position of the benzylcarbonyl subunit and the R_2, R_4 and R_6 positions of the naphthyl ring, favorable to the introduction of electron-rich groups. In conclusion, structural variation around these positions may be modulating selectivity towards CB2 receptor subtype.

The statistical values obtained from the best CoMFA model of selectivity for CB2, as well as the correlation of the experimental selectivity obtained using the CB2/CB1 p*K*i ratio *versus* predicted p*K*i, are presented in Tables 5 and 6. The plot of CoMFA steric/electrostatic selectivity model for CB2 showing the selectivity values obtained experimentally for the ligands from the training and test sets correlated to their predicted values is presented in Fig. 13.

As we had done in the CoMFA analysis, in the CoMSIA analysis we built models using CB1/CB2 CB2/CB1 p*K*i ratio, with the goal of checking if there was a qualitative reversal of the hydrophobic contour maps (Fig. 14) that could help design selective CB1 or CB2 ligands based on that property.

As observed in the CoMFA analysis and construction of selectivity models for CB1/CB2 and CB2/CB1, the visual inspection of the hydrophobic contour maps revealed inverted fields (Fig. 14a and b). In the hydrophobic contour map for CB1 (Fig. 14a), the same two compounds described in CoMFA selectivity models are illustrated: JWH-081 (**9**) and JWH-265 (**43**) being the highest and second lowest selectivity for CB1/CB2, respectively.

The oxygen atom present in the methoxy group at R_4 position of the naphthyl ring of the ligand JWH-081 (**9**) is close to a region of the hydrophobic contour map where the presence of polar groups increases the selectivity towards CB1. On the contrary, with JWH-

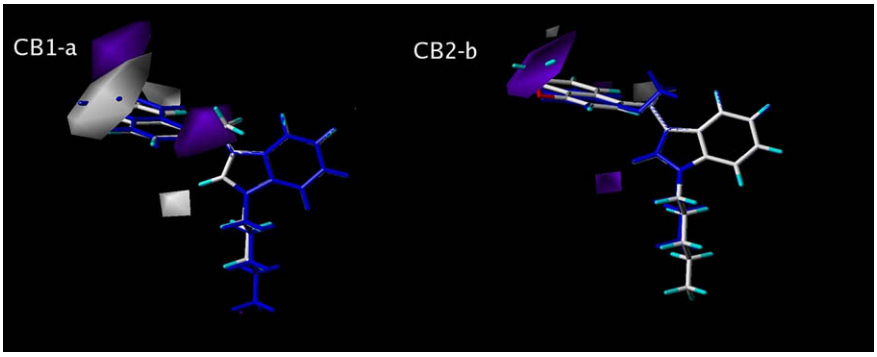

Fig. 14. CoMSIA hydrophobic contour maps of selectivity. (a) Compounds JWH-081, in blue, and JWH-265 for CB1 and (b) JWH-265, in blue, and JWH-081 for CB2 are shown inside fields. Purple regions (80% contribution) indicate areas where hydrophobic groups increase activity and white regions (20% contribution) indicate areas where hydrophobic groups decrease activity. (For interpretation of the references to colour in this figure legend, the reader is referred to the web version of this article.)

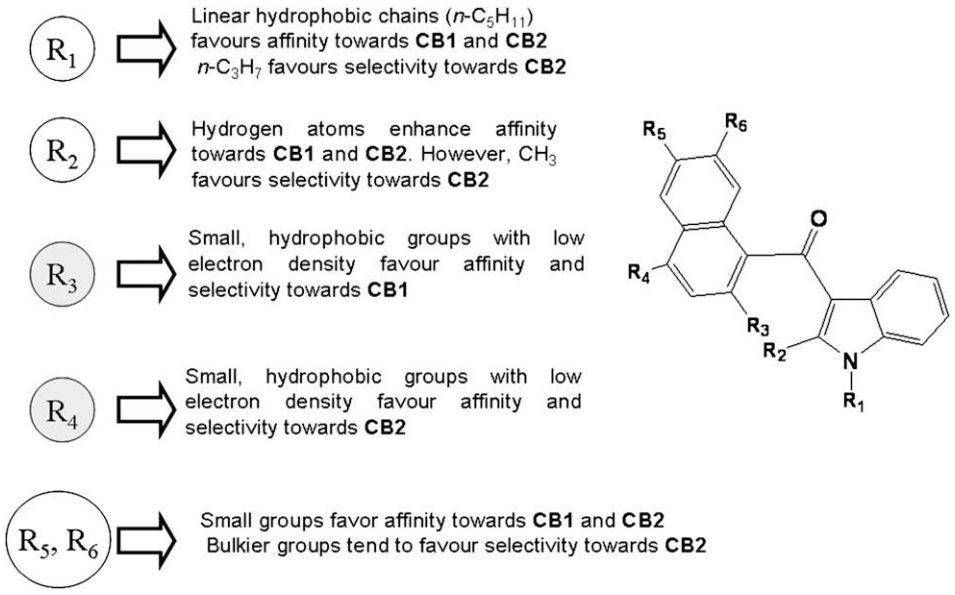

Fig. 15. Structure–affinity/selectivity relationships derived from CoMFA/CoMSIA 3D-QSAR studies developed in this work.

265 (**43**) the oxygen atom of the methoxy group in R_3 position of the naphthyl ring is close to a region of the hydrophobic contour map which is unfavorable to polar groups. This result, in conjunction to all the other analyses, emphasizes again that the substitution pattern in the R_2 position of the indole ring may be modulating ligand selectivity towards CB2 (Fig. 14b), as well as the presence of hydrophobic or hydrophilic substituents in the R_2 and R_4 positions of the naphthyl ring, respectively.

The statistical values obtained from the best CoMSIA model of selectivity for CB2, as well as the correlation of the experimental selectivity obtained using the CB2/CB1 p*K*i ratio *versus* predicted p*K*i, are presented in Tables 5 and 6.

Finally, the work presented herein enabled us to propose the stereoelectronic regions affecting both affinity and selectivity towards CB1 and CB2 (Fig. 15), which may be relevant for the design of new indole derivatives selective towards CB1 or CB2 with good potency and with a safer pharmacotherapeutic profile.

4. Concluding remarks

In the present study, we examined the 3D-QSAR models (CoMFA and CoMSIA) of affinity and selectivity of a set of CB1 and CB2 ligands belonging to the indole class. The models have proven to be statistically robust, with average q^2 of 0.675 and average r^2 of 0.855. Also, as demonstrated in our study, the developed steric/electrostatic and hydrophobic models helped us to understand the structural features responsible for the affinity and selectivity of the indole ligands for both CB1 and CB2 receptors and the discussion enabled us to propose the stereoelectronic regions affecting these profiles. Finally, the work may be considered as a powerful tool in the design of new safer and therapeutically useful structurally related cannabinoid ligand drugs. It is worth to note the fact that selectivity assessment for these two receptor subtypes has not been reported in the literature *prior* to our work.

Acknowledgements

The authors thank CNPq (Br), FAPERJ (Br), PRONEX-2006 (Br), and IM-INOFAR (Br, #420.015/05-1) for the financial support and fellowships (to G.B.L., N.C.R. and C.A.M.F.).

References

[1] A.C. Howlett, F. Barth, T.I. Bonner, G. Cabral, P. Casellas, W.A. Devane, C.C. Felder, M. Herkenham, K. Mackie, B.R. Martin, R. Mechoulam, R.G. Pertwee, Pharmacol. Rev. 54 (2002) 161–202.
[2] A.J. Brown, Br. J. Pharmacol. 152 (2007) 567–575.
[3] H.A. Overton, A.J. Babbs, S.M. Doel, M.C.T. Fyfe, L.S. Gardner, G. Griffin, H.C. Jackson, M.J. Procter, C.M. Rasamison, M. Tang-Christensen, P.S. Widdowson, G.M. Williams, C. Reynet, Cell Metab. 3 (2006) 167–175.
[4] L.A. Matsuda, S.J. Lolait, M.J. Brownstein, A.C. Young, T.I. Bonner, Nature 346 (1990) 561–564.
[5] J.W. Huffman, J.A.H. Lainton, Curr. Med. Chem. 3 (1996) 101–116.
[6] R.G. Pertwee, Curr. Med. Chem. 6 (1999) 635–664.
[7] S. Galiegue, S. Mary, J. Marchand, D. Dussossoy, D. Carriere, P. Carayon, M. Bouaboula, D. Shire, G. Le Fur, P. Casellas, Eur. J. Biochem. 232 (1995) 54–61.
[8] A. Wise, K. Gearing, S. Rees, Drug Discov. Today 7 (2002) 235–246.
[9] P.H. Reggio, Curr. Pharm. Des. 9 (2003) 1607–1633.
[10] C.C. Felder, K.E. Joyce, E.M. Briley, J. Mansouri, K. Mackie, O. Blond, Y. Lai, A.L. Ma, R.L. Mitchell, Mol. Pharmacol. 48 (1995) 443–450.
[11] T. Tuccinardi, P.L. Ferrarini, C. Manera, G. Ortore, G. Saccomanni, A. Martinelli, J. Med. Chem. 49 (2006) 984–994.
[12] R.G. Pertwee, Prog. Neurobiol. 63 (2001) 569–611.
[13] R.G. Pertwee, Pharmacol. Ther. 95 (2002) 165–174.
[14] R.G. Pertwee, Addiction 94 (1999) 317–320.
[15] R.G. Pertwee, Addict. Biol. 5 (2000) 37–46.
[16] D. Piomelli, A. Giuffrida, A. Calignano, F. Rodriguez de Fonseca, Trends Pharmacol. Sci. 21 (2000) 218–224.
[17] M.E. Abood, B.R. Martin, Trends Pharmacol. Sci. 13 (1992) 201–206.
[18] M. Rinaldi-Carmona, F. Barth, M. Héaulme, D. Shire, B. Calandra, C. Congy, S. Martinez, J. Maruani, G. Néliat, D. Caput, P. Ferrara, P. Soubrié, J.C. Brelière, G. Le Fur, FEBS Lett. 350 (1994) 240–244.
[19] Z.H. Song, T.I. Bonner, Mol. Pharmacol. 49 (1996) 891–896.
[20] S.D. McAllister, G. Rizvi, S. Anavi-Goffer, D.P. Hurst, J. Barnett-Norris, D.L. Lynch, P.H. Reggio, M.E. Abood, J. Med. Chem. 46 (2003) 5139–5152.
[21] Z.H. Song, C.A. Slowey, D.P. Hurst, P.H. Reggio, Mol. Pharmacol. 56 (1999) 834–840.
[22] J.Y. Shim, E.R. Collantes, W.J. Welsh, B. Subramaniam, A.C. Howlett, M.A. Eissenstat, S.J. Ward, J. Med. Chem. 41 (1998) 4521–4532.
[23] A.R. Keimowitz, B.R. Martin, R.K. Razdan, P.J. Crocker, S.W. Mascarella, B.F. Thomas, J. Med. Chem. 43 (2000) 59–70.
[24] M.E.Y. Francisco, H.H. Seltzman, A.F. Gilliam, R.A. Mitchell, S.L. Rider, R.G. Pertwee, L.A. Stevenson, B.F. Thomas, J. Med. Chem. 45 (2002) 2708–2719.
[25] S. Durdagi, A. Kapou, T. Kourouli, T. Andreou, S.P. Nikas, V.R. Nahmias, D.P. Papahatjis, M.G. Papadopoulos, T. Mavromoustakos, J. Med. Chem. 50 (2007) 2875–2885.
[26] J.Y. Shim, W.J. Welsh, E. Cartier, J.L. Edwards, A.C. Howlett, J. Med. Chem. 45 (2002) 1447–1459.
[27] J.Z. Chen, X.W. Han, Q. Liu, A. Makriyannis, J. Wang, X.Q. Xie, J. Med. Chem. 49 (2006) 625–636.
[28] O.M.H. Salo, J.R. Savinainen, T. Parkkari, T. Nevalainen, M. Lahtela-Kakkonen, J. Gynther, J.T. Laitinen, T. Järvinen, A. Poso, J. Med. Chem. 49 (2006) 554–566.
[29] M. Fichera, G. Cruciani, A. Bianchi, G. Musumarra, J. Med. Chem. 43 (2000) 2300–2309.

[30] S. Durdagi, M.G. Papadopoulos, D.P. Papahatjis, T. Mavromoustakos, Bioorg. Med. Chem. Lett. 17 (2007) 6754–6763.
[31] W. Tong, E.R. Collantes, W.J. Welsh, J. Med. Chem. 41 (1998) 4207–4215.
[32] J.Y. Shim, A.C. Howlett, J. Chem. Inf. Model. 46 (2006) 1286–1300.
[33] C. Montero, N.E. Campillo, P. Goya, J.A. Páez, Eur. J. Med. Chem. 40 (2005) 75–83.
[34] O.M.H. Salo, M. Lahtela-Kakkonen, J. Gynther, T. Järvinen, A. Poso, J. Med. Chem. 47 (2004) 3048–3057.
[35] J.W. Huffman, G. Zengin, M.J. Wu, J. Lu, G. Hynd, K. Bushell, A.L.S. Thompson, S. Bushell, C. Tartal, D.P. Hurst, P.H. Reggio, D.E. Selley, M.P. Cassidy, J.L. Wiley, B.R. Martin, Bioorg. Med. Chem. 13 (2005) 89–112.
[36] J.W. Huffman, P.V. Szklennik, A. Almond, K. Bushell, D.E. Selley, H. He, M.P. Cassidy, J.L. Wiley, B.R. Martin, Bioorg. Med. Chem. Lett. 15 (2005) 4110–4113.
[37] L.W. Padgett, Life Sci. 77 (2005) 1767–1798.
[38] D.R. Compton, K.C. Rice, B.R. De Costa, R.K. Razdan, L.S. Melvin, M.R. Johnson, B.R. Martin, J. Pharmacol. Exp. Ther. 265 (1993) 218–226.
[39] V.M. Showalter, D.R. Compton, B.R. Martin, J. Pharmacol. Exp. Ther. 278 (1996) 989–999.
[40] SPARTAN PRO version 1.0.5, Wavefunction Inc., 18401 Von Karman Avenue, Suite 370 Irvine, CA 92612, USA, 2006.
[41] T.A. Halgren, J. Am. Chem. Soc. 112 (1990) 4710–4723.
[42] SYBYL version 7.3, Tripos Inc., 1699 South Hanley Road, St. Louis, MO 63144, USA, 2007.
[43] M. Akamatsu, Curr. Top. Med. Chem. 12 (2002) 1381–1394.
[44] R.D. Cramer, J. Am. Chem. Soc. 110 (1988) 5959–5967.